

POSSIBLE EVIDENCE FOR METAL ACCRETION ONTO THE SURFACES OF METAL-POOR MAIN-SEQUENCE STARS

KOHEI HATTORI¹, YUZURU YOSHII¹, TIMOTHY C. BEERS^{2,3}, DANIELA CAROLLO^{4,5}, AND YOUNG SUN LEE⁶

Draft version February 19, 2014

ABSTRACT

The entire evolution of the Milky Way, including its mass-assembly and star-formation history, is imprinted onto the chemo-dynamical distribution function of its member stars, $f(x, v, [X/H])$, in the multi-dimensional phase space spanned by position, velocity, and elemental abundance ratios. In particular, the chemo-dynamical distribution functions for low-mass stars (e.g., G- or K-type dwarfs) are precious tracers of the earliest stages of the Milky Way's formation, since their main-sequence lifetimes approach or exceed the age of the universe. A basic tenet of essentially all previous analyses is that the stellar metallicity, usually parametrized as $[Fe/H]$, is conserved over time for main-sequence stars (at least those that have not been polluted due to mass transfer from binary companions). If this holds true, any correlations between metallicity and kinematics for long-lived main-sequence stars of different masses, effective temperatures, or spectral types must strictly be the same, since they reflect the same mass-assembly and star-formation histories. By analyzing a sample of nearby metal-poor halo and thick-disk stars on the main sequence, taken from Data Release 8 of the Sloan Digital Sky Survey, we find that the median metallicity of G-type dwarfs is systematically higher (by about 0.2 dex) than that of K-type dwarfs having the same median rotational velocity about the Galactic center. If it can be confirmed, this finding may invalidate the long-accepted assumption that the atmospheric metallicities of long-lived stars are conserved over time.

Subject headings: Galaxy: evolution — Galaxy: formation — Galaxy: halo — Galaxy: kinematics and dynamics — stars: abundances

1. INTRODUCTION

Numerical calculations of the nuclear processes that take place in stellar interiors have established that the evolutionary track of a given star is determined primarily by two parameters – its mass and chemical composition (other parameters, such as stellar rotation and magnetic fields may play roles as well, but they are expected to be smaller). While main-sequence stars are believed to retain the initial values of their mass and composition from birth through the completion of core H burning, it has been conjectured previously that this may not necessarily be the case, depending on their surrounding environment. For example, Bondi (1952) demonstrated, from theoretical considerations, that a star can accrete gas onto its surface at a rate proportional to v_{rel}^{-3} , where v_{rel} is the relative velocity between the star and the gas with which it collides. In particular, if initially metal-poor stars accrete metal-rich gas, this would lead to an enhancement of the metallicity in their atmospheres, and thus confound a straightforward interpretation of the chemical evolution of the Galaxy.

Yoshii (1981) was the first to speculate that Bondi mass accretion onto halo stars may drastically alter their surface metal abundances in the course of formation of the Galactic halo, proposing that more metal-poor halo stars would suffer greater surface metal enhancements than metal-rich stars, due to their shallower surface convective envelopes. He argued that, early in the formation history of the Milky Way, before the emergence of the disk, gaseous material is primarily distributed throughout the halo. During this era, high-density gas clouds move more or less randomly throughout the halo. If halo stars formed from these clouds, it is possible for them to collide at small relative velocity with chemically processed dense gas from previous star-formation episodes in these same clouds, so that mass accretion as well as surface metal enhancement is likely to occur. After the halo gas has contracted to form the disk stellar populations, mass accretion onto halo stars becomes negligible, for two reasons. First, halo stars collide with dense gas only occasionally, when they pass through the disk. Secondly, such collisions occur near the pericenter of the stellar orbits, hence the relative velocity between halo stars and the disk gas is too large to enable efficient mass accretion.

According to the currently favored hierarchical galaxy formation paradigm in a Λ -CDM universe, the Galaxy is thought to form through mergers of sub-galactic systems for which the internal velocity dispersion is much smaller than that of the ensemble of these systems that make up the entire halo (see, e.g., Tissera et al. 2013, and references therein). Because the relative velocity between the stars and the gas within these systems is on the order of their internal velocity dispersions, this scenario implicitly involves conditions that are favorable for mass accretion,

khattori@ioa.s.u-tokyo.ac.jp

¹ Institute of Astronomy, School of Science, University of Tokyo, 2-21-1, Osawa, Mitaka, Tokyo 181-0015, Japan

² National Optical Astronomy Observatories, Tucson, AZ 85719, USA

³ JINA: Joint Institute for Nuclear Astrophysics

⁴ Macquarie University - Dept. Physics & Astronomy, Sydney, 2109 NSW, Australia

⁵ INAF - Osservatorio Astronomico di Torino, 10025 Pino Torinese, Torino - Italy

⁶ Department of Astronomy, New Mexico State University, Las Cruces, NM 88003, USA

as suggested years ago by Yoshii (1981).

Several previous authors have attempted to evaluate the rate of mass accretion in a cosmological context, and reached similar conclusions, that the surface metal abundances of low-mass, initially metal-poor (or even near zero-metallicity stars) could indeed be enhanced significantly (e.g., Shige-yama et al. 2003; Komiya et al. 2010). Other authors have argued against the notion that significant mass accretion onto halo stars could have occurred. For example, Frebel et al. (2009) calculated the orbits of individual halo stars in order to evaluate the amount of mass that might have been accreted as they penetrate the disk (several times over the age of the Galaxy), and concluded that their surface metal abundances are hardly enhanced. However, in this work, the amount of mass accreted by individual stars within their natal sub-galactic systems, which may be the dominant source, is not taken into account.

In order to break this stalemate, we propose an observational test to decide whether or not the accretion hypothesis may indeed be supported. Suppose that metal-poor halo G- and K-type dwarfs, with main-sequence lifetimes close to or exceeding the age of the universe, experience no mass accretion and associated surface metallicity enhancement, and that their kinematical properties are independent of spectral type, because they share the same star-formation and mass-assembly histories. Then, any observed correlation between metallicity and kinematics for G-type dwarfs must be identical to that observed for K-type dwarfs. However, if mass accretion and metallicity enhancement did occur, the situation is expected to be quite different. According to theoretical studies of the internal structures of stars, the mass of the surface convective envelope for dwarfs drastically decreases with increasing effective temperature, T_{eff} . This implies that the affect of surface metal enhancement on G-type dwarfs is expected to be much larger than for K-type dwarfs (due to the lack of dilution in their surface layers), even if they had the same initial metal abundance and the same amount of mass accreted. Thus, we can accept or reject the accretion hypothesis by examining whether a spectral-type dependent shift in metallicity for stars with otherwise identical kinematics exists or not.

Note that this test is possible only statistically, based on a large, kinematically unbiased sample of metal-poor main-sequence dwarfs. In this paper, we employ spectroscopic observations of G- and K-type dwarfs in a relatively local region of the halo, taken from Data Release 8 of the Sloan Digital Sky Survey (SDSS DR8, Aihara et al. 2011), to derive the relation between the median rotational velocity, $\langle V_{\phi} \rangle_{\text{med}}$, and the surface metal abundance, $[\text{Fe}/\text{H}]$, for stars of different spectral types. If the above mentioned shift in metallicity with respect to kinematics is confirmed, it would be the first observational evidence of the importance of mass accretion onto halo stars. Given the implications of this, and the clear influence on the interpretation of future observations, it is crucial to seek confirmation (or refutation) based on additional studies.

This paper is organized as follows. We describe our sample selection in Section 2, and present our analysis and results in Section 3. The plausibility of our results is discussed in Section 4. Our interpretation of these

results is presented in Section 5. Finally, in Section 6 we summarize our results, and suggest future tests of this hypothesis.

2. SAMPLE

In this section, we describe how we construct a kinematically unbiased sample of low-mass main-sequence stars based on SDSS DR8.

2.1. Target Selection

The spectroscopic samples in SDSS, as well as in its stellar-specific sub-surveys, the Sloan Extension for Galactic Understanding and Exploration (SEGUE-1; Yanny et al. 2009) and SEGUE-2 (Rockosi et al., in preparation) are selected (targeted) based on a series of photometric (magnitude and color) and/or proper-motion cuts. In order to construct a kinematically unbiased sample, we avoid using stars whose target criteria includes any proper-motion cuts. Since the target criteria for stars in the different surveys are not identical, we first examined their detailed descriptions to determine which might be best used for our present purpose. After some consideration, from SDSS we include only those objects targeted as *BHB candidates* (a subset of these are used for a separate test below). From SEGUE-1, we select those objects whose target names are either *K-dwarf candidates*, *G-dwarf candidates*, or *low-metallicity candidates*. We do not select any objects from the SEGUE-2 sub-survey. The combined sample comprises the basis for our subsequent analysis. Note that our sample is based initially on the target criterion, not on how the star was classified after its spectrum was obtained.

2.2. Selection of G/K-type dwarfs with Reliable Stellar Parameters and Kinematics

In order to construct a sample of low-mass, main-sequence dwarfs with reliable estimates of atmospheric metallicity, $[\text{Fe}/\text{H}]$, 3-D positions, and space motions, we further restrict our selection to meet additional criteria. In this process, we make use of the stellar parameters derived from the most recent version of the SEGUE Stellar Parameter Pipeline (SSPP; see Lee et al. 2008a,b; Allende Prieto et al. 2008; Smolinski et al. 2011). Note that the SSPP metallicity estimate is optimized for low-mass dwarfs, in essentially the same way as in Schlesinger et al. (2012).

First, from the above-mentioned stellar sample, we select stars with $S/N > 20$ per 1 Å pixel, colors in the range $0.48 < (g-r)_0 < 0.75$, derived surface gravity $\log g > 4.1$, and effective temperatures in the range $4500 \text{ K} < T_{\text{eff}} < 6000 \text{ K}$. Here, $(g-r)_0$ is the reddening-corrected $(g-r)$ color based on application of the prescription by Schlegel et al. (1998). The lower limit on the S/N ratio ensures that errors in $[\text{Fe}/\text{H}]$ derived by the SSPP are not too large (typically smaller than 0.15 dex; Allende Prieto et al. 2008). The lower limit on $\log g$ is set to reliably include dwarf stars. The upper and lower limits on effective temperature T_{eff} correspond to G0 and K4, respectively (Habets & Heintze 1981)⁷. We then select those stars with one-sigma errors in line-of-sight ve-

⁷ Note that the MK system is defined for solar-metallicity stars, so these ranges on spectral type only loosely apply to low-metallicity stars.

locity, v_{los} , smaller than 20 km s^{-1} , and with one-sigma proper-motion errors motion smaller than 5 mas yr^{-1} .

2.3. Construction of a Volume-Limited Sample

In order to approximate a sample that reflects the nature of a volume-limited sample, we retain stars with absorption-corrected r_0 magnitudes in the range $15 < r_0 < 18.45$. Then, we select those stars with heliocentric distances, d , in the range $0.84 \text{ kpc} < d < 1.64 \text{ kpc}$, and with atmospheric metallicities in the range $-2.0 < [\text{Fe}/\text{H}] < -0.5$, as derived by the SSPP (Beers et al. 2012). These distance and metallicity ranges are designed to ensure that the G- and K-type dwarfs fairly explore the same volume (that is, we seek to avoid populating the volume differently for the two spectral types), based on the set of 10 Gyr model isochrones described in An et al. (2009). Then, we divide our sample stars into G- and K-dwarf samples based on T_{eff} . Throughout this paper, those dwarfs with $5250 \text{ K} < T_{\text{eff}} < 6000 \text{ K}$ are referred to as G-type dwarfs, which (for solar-abundance stars) corresponds to G0-G9 (Habets & Heintze 1981), while those with $4500 \text{ K} < T_{\text{eff}} \leq 5250 \text{ K}$ are referred to as K-type dwarfs, which correspond to K0-K4 (for solar-abundance stars). Our final sample consists of 7124 G-type dwarfs and 3257 K-type dwarfs.

The mean distances of the two samples, $1.263 \pm 0.003 \text{ kpc}$ (G-type dwarfs) and $1.254 \pm 0.004 \text{ kpc}$ (K-type dwarfs) are quite close to one another. A two-sample Kolmogorov-Smirnov test of the distributions of heliocentric distance for the G- and K-dwarf samples is unable to reject the null hypothesis that they are drawn from the same parent distribution. The p -value of the test (0.081) is larger than the widely adopted threshold of 0.05; we conclude that the spatial distributions for these two samples do not significantly differ.

2.4. Caveats on a Metallicity Selection Bias

We are aware that our sample is affected by a selection bias in which more metal-poor stars are preferentially observed (see section 4.7 of Schlesinger et al. 2012). Such a selection bias must be treated with care if we are concerned with extracting the metallicity distribution functions for stars in our sample. However, this metallicity-dependent selection bias should not impact our derivation of the median rotational velocity (V_ϕ in a cylindrical system) for stars at a given *fixed* metallicity, since it does not depend on *how many* sample stars are used. In the following, we compare the relationship between $\langle V_\phi \rangle_{\text{med}}$ – by which we indicate the median rotational velocity – and $[\text{Fe}/\text{H}]$ for different stellar subsamples.

3. MEDIAN ROTATIONAL VELOCITY AS A FUNCTION OF METALLICITY

3.1. Kinematical Information

In this paper we assume that the Local Standard of Rest (LSR) is on a circular orbit with a rotation speed of 220 km s^{-1} (Kerr & Lynden-Bell 1986; Bovy et al. 2012), and that the Galactocentric distance of the Sun is $R_\odot = 8.5 \text{ kpc}$ (Ghez et al. 2008; Koposov et al. 2010). We also assume that the peculiar motion of the Sun with respect to the LSR is $(U_\odot, V_\odot, W_\odot) = (10.0, 5.3, 7.2) \text{ km s}^{-1}$ (Dehnen & Binney 1998).

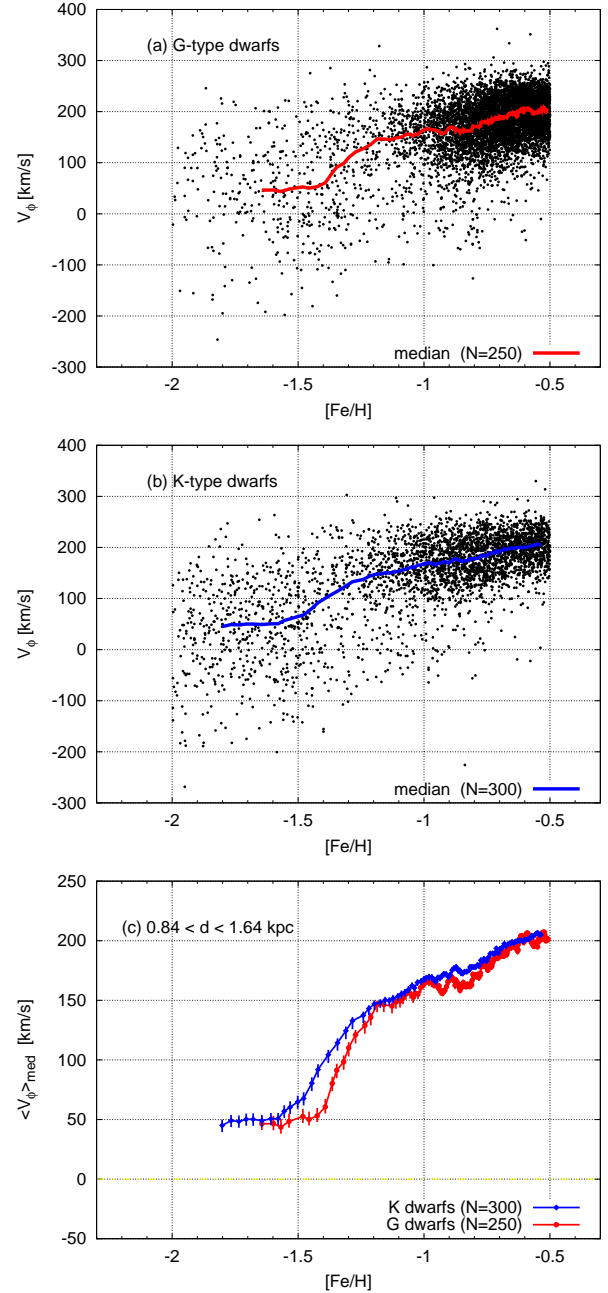


FIG. 1.— Distribution of our sample stars in the V_ϕ - $[\text{Fe}/\text{H}]$ space and the median value of V_ϕ for binned samples in the metallicity range $-2.0 < [\text{Fe}/\text{H}] < -0.5$. (a) Results for G-type dwarfs. We bin $N = 250$ stars sorted in $[\text{Fe}/\text{H}]$, moving through the sample in steps of $N/10$ stars, and show the median value of V_ϕ (or $\langle V_\phi \rangle_{\text{med}}$) at the median value of $[\text{Fe}/\text{H}]$. (b) Results for K-type dwarfs. The analysis is the same as in (a), but adopting $N = 300$ instead. (c) Comparison of the median values $\langle V_\phi \rangle_{\text{med}}$ for G- and K-type dwarfs. Error bars in $\langle V_\phi \rangle_{\text{med}}$ are estimated by assuming a Gaussian-like distribution of V_ϕ .

With these assumptions, and the available estimated distances, line-of-sight velocities, and proper motions, we calculate the 3-D positions and space motions of our sample stars. Noting that the fractional error in the SSPP distance is around 10-20%, and that the typical error in line-of-sight velocity and proper motion is around 2 km s^{-1} and 3.5 mas yr^{-1} , respectively, the associated er-

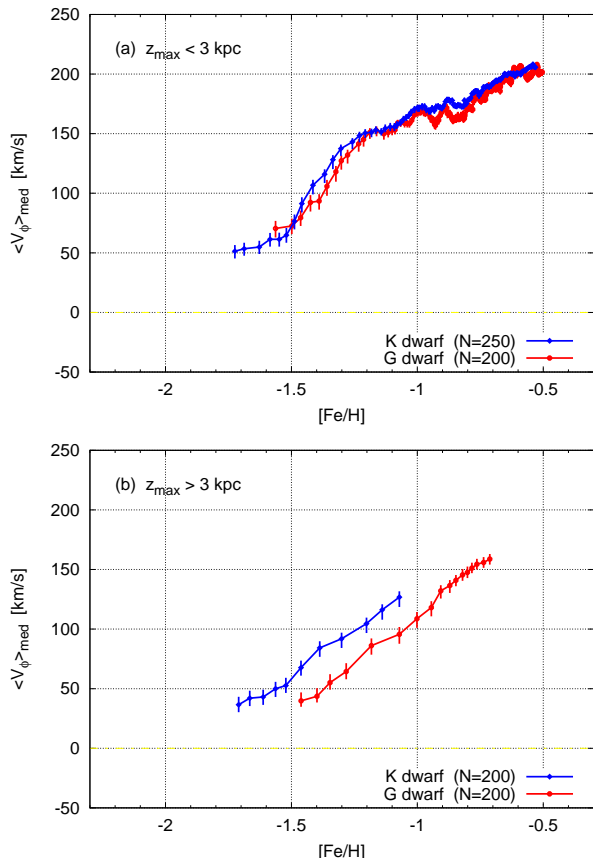


FIG. 2.— Median value of V_ϕ as a function of $[\text{Fe}/\text{H}]$ for G-type dwarf (red) and K-type dwarf (blue) subsamples having different ranges of z_{max} (maximum orbital excursion perpendicular to the Galactic disk plane). The results for sample stars with $z_{\text{max}} < 3$ kpc and $z_{\text{max}} > 3$ kpc are shown in panels (a) and (b), respectively. The binning procedure is the same as in Figure 1, and the adopted value of bin size N for each subsample is shown on the panel.

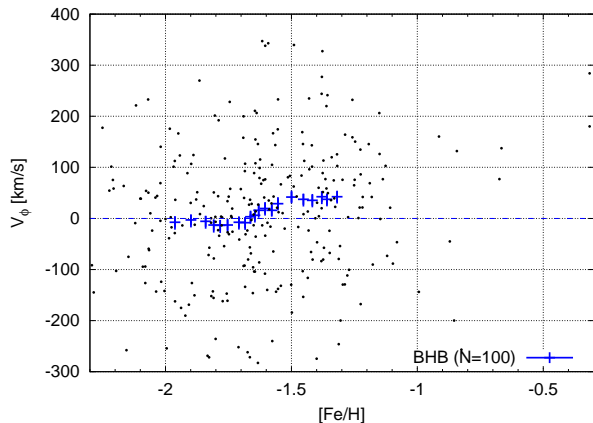


FIG. 3.— The distribution in the V_ϕ - $[\text{Fe}/\text{H}]$ space of BHB stars with $5 \text{ kpc} < R < 20 \text{ kpc}$ and $2 \text{ kpc} < |z| < 5 \text{ kpc}$. Also shown is the median value, $\langle V_\phi \rangle_{\text{med}}$, for the binned sample. The binning procedure is the same as in Figure 1, but by binning $N = 100$ stars and moving through each sample in steps of $N/10$ stars. The associated error bar on $\langle V_\phi \rangle_{\text{med}}$ represents the uncertainty estimated by assuming a Gaussian-like distribution of V_ϕ .

ror in each of the velocity components of our sample stars is typically around 30-40 km s^{-1} .

3.2. Median Rotational Velocity Behavior with $[\text{Fe}/\text{H}]$

Panels (a) and (b) of Figure 1 show the distribution of G and K-type dwarfs, respectively, in the V_ϕ - $[\text{Fe}/\text{H}]$ space. In each panel, a solid line indicates the running median $\langle V_\phi \rangle_{\text{med}}$ as a function of $[\text{Fe}/\text{H}]$, sweeping through the sample with overlapping bins of N stars sorted in $[\text{Fe}/\text{H}]$ (with an overlap of $0.9N$ stars per bin), using $N = 250$ G-type dwarfs and $N = 300$ K-type dwarfs. Panel (c) of Figure 1 compares the two distributions, with an associated error in $\langle V_\phi \rangle_{\text{med}}$ estimated by assuming a Gaussian-like distribution of V_ϕ . For both the G- and K-dwarf samples, we note a gradual transition from a nearly non-rotating, halo-dominated region at $[\text{Fe}/\text{H}] < [\text{Fe}/\text{H}]_{\text{knee}} \simeq -1.5$ to a rapidly-rotating, thick-disk dominated region at $[\text{Fe}/\text{H}] \gtrsim -1.0$.⁸ However, we also note that there appears to be a systematic offset in the $\langle V_\phi \rangle_{\text{med}}$ - $[\text{Fe}/\text{H}]$ relation between the G- and K-type dwarfs, such that the offset in $[\text{Fe}/\text{H}]$ increases as $\langle V_\phi \rangle_{\text{med}}$ decreases. The offset in $[\text{Fe}/\text{H}]$ (when $\langle V_\phi \rangle_{\text{med}}$ is fixed) increases as a function of $\langle V_\phi \rangle_{\text{med}}$, from $\delta = 0.05$ dex at $\langle V_\phi \rangle_{\text{med}} \simeq 150 \text{ km s}^{-1}$ to $\delta = 0.20$ dex at $\langle V_\phi \rangle_{\text{med}} \simeq 50 \text{ km s}^{-1}$, below which the $\langle V_\phi \rangle_{\text{med}}$ - $[\text{Fe}/\text{H}]$ relation becomes flat. In other words, the offset becomes larger in the more metal-poor, and therefore more halo-dominated region.

It is also intriguing to note that the offset becomes milder at $\langle V_\phi \rangle_{\text{med}} > 150 \text{ km s}^{-1}$, where the contribution from the thick disk becomes larger, and that the offset becomes invisible at $\langle V_\phi \rangle_{\text{med}} > 170 \text{ km s}^{-1}$ or $[\text{Fe}/\text{H}] > -0.8$, where the sample is dominated by thick-disk stars.

We note here the possibility that some perturbative mechanisms (such as close encounters with giant molecular clouds in the disk plane) could result in a mass segregation of disk stars, and produce a difference in the $\langle V_\phi \rangle_{\text{med}}$ - $[\text{Fe}/\text{H}]$ relation. We check this possibility using a simple mass distribution model for the Milky Way, and find that the difference in the stellar masses of G- and K-type dwarfs is too small to cause the observed offset of 30-40 km s^{-1} at $[\text{Fe}/\text{H}] \simeq -1.4$. Therefore, hereafter we interpret the detected offset in $\langle V_\phi \rangle_{\text{med}}$ - $[\text{Fe}/\text{H}]$ relation as an offset in $[\text{Fe}/\text{H}]$, not as one in $\langle V_\phi \rangle_{\text{med}}$.

Next, we derive the orbital parameters for each of the sample stars, assuming the Stäckel-type gravitational potential of the Milky Way adopted by Chiba & Beers (2001). We divide our G- and K-dwarf samples according to whether z_{max} is larger or smaller than 3 kpc (z_{max} denotes the largest orbital excursion perpendicular to the Galactic disk plane achieved by a given star during its orbit), and perform the same analysis as carried out above.

Panels (a) and (b) in Figure 2 show the median value of V_ϕ , as a function of $[\text{Fe}/\text{H}]$, for our sample stars with $z_{\text{max}} < 3 \text{ kpc}$ and $z_{\text{max}} > 3 \text{ kpc}$, respectively. The binning procedure is the same as used for Figure 1, with the N employed shown on each panel. Although the offset in $\langle V_\phi \rangle_{\text{med}}$ - $[\text{Fe}/\text{H}]$ relation is not clear in panel (a), it becomes very apparent in panel (b). The magnitude of the

⁸ Note that most of our sample stars are located more than 0.5 kpc away from the disk plane, while the scale heights of thin- and thick-disk components are around 0.25-0.35 kpc and 0.7-1.2 kpc, respectively (Yoshii 1982; Gilmore & Reid 1983; Yoshii 2013).

offset on panel (b) is $\delta \simeq 0.20$ dex, which is as large as the maximum offset seen in Figure 1.

4. PLAUSIBILITY OF OUR RESULTS

In section 3, we find that G- and K-type dwarfs show different behaviour in the $\langle V_\phi \rangle_{\text{med}} - [\text{Fe}/\text{H}]$ relation. Here we discuss how the selection bias in SDSS or observational errors may affect our results and investigate the plausibility of our results.

4.1. Selection Bias in SDSS

Schlesinger et al. (2012) point out that, even if they take into account the metallicity-dependent selection bias inherent in SDSS/SEGUE, the fraction of metal-poor K-type dwarfs is larger than that of G-type dwarfs, especially in the high $|z|$ -region ($|z|$ is the distance from the Galactic disk plane). In order to investigate if this discrepancy is involved with producing the observed offset in the $\langle V_\phi \rangle_{\text{med}} - [\text{Fe}/\text{H}]$ relation, we select those sample stars that appear also in the Schlesinger et al. (2012) sample, and check the $|z|$ -dependence of the $\langle V_\phi \rangle_{\text{med}} - [\text{Fe}/\text{H}]$ relation. We find that the offset can be confirmed independent of $|z|$, which suggests that the observed offset is not relevant to the discrepancy found in Schlesinger et al. (2012).

4.2. Observational Errors

4.2.1. Systematic Errors in SSPP Metallicity Estimates

The simplest explanation of our finding that G- and K-type dwarfs show different $\langle V_\phi \rangle_{\text{med}} - [\text{Fe}/\text{H}]$ relations is that it is due to a temperature-related systematic error in the determination of $[\text{Fe}/\text{H}]$ by the SSPP. If such a systematic error in $[\text{Fe}/\text{H}]$ exists, we may detect a systematic difference between SSPP metallicity and the metallicity derived from high-resolution spectroscopy for G/K-type dwarfs. We check this possibility by using five G-type dwarfs and two K-type dwarfs taken from Table 4 of Allende Prieto et al. (2008), and find that G-type dwarfs tend to have ~ 0.2 dex higher SSPP metallicity than the high-resolution metallicity, while the two estimates of metallicity more or less agree with each other for K-type dwarfs.⁹ Although the sample size (in total seven) is insufficient to be confident, the uncertainty in SSPP metallicity might influence the observed offset in $\langle V_\phi \rangle_{\text{med}} - [\text{Fe}/\text{H}]$ relations in Figure 1 or 2.

However, if the apparent offset in Figure 1 is due to a spectral-type dependent systematic error in the SSPP metallicity, we would also expect a similar offset in Figure 2(a). The fact that we see a clear offset only in Figure 1 and 2(b) and not in Figure 2(a), may indicate that the existence or non-existence of the offset in the $\langle V_\phi \rangle_{\text{med}} - [\text{Fe}/\text{H}]$ relation in these figures is real. This notion is supported by the mock data analysis presented in section 4.2.4.

4.2.2. Random Errors in Proper Motion

⁹ According to Allende Prieto et al. (2008), possible systematic errors in $[\text{Fe}/\text{H}]$ for SDSS/SEGUE spectra with $S/N > 20$ are less than 0.15 dex. However, this value does not directly apply to our sample dwarfs, since their sample includes not only dwarfs but also more luminous giants. Indeed, their Table 4 indicates that the uncertainty in the SSPP metallicity for G/K-type dwarfs might be as large as 0.3 dex.

The largest contribution to the uncertainty in the measured velocity components of our sample stars arises from the observational errors in proper motion, which are typically as large as 3.5 mas yr^{-1} . However, the proper-motion error does not seem to affect the median value, $\langle V_\phi \rangle_{\text{med}}$, since it is a purely random error in most cases. In order to estimate the effect of proper-motion errors on our results, we first construct 100 error-added samples of G- and K-type dwarfs. To do this, we randomly add/subtract an error term to the observed proper motion that obeys a Gaussian distribution with standard deviation corresponding to the one-sigma observational error in the proper motion. Then, we perform the same analysis to these error-added samples, and compare the results with that of the as-observed sample. After these calculations, we confirm that the proper-motion error scarcely affects our results shown in Figure 1 or 2.

4.2.3. Systematic Errors in SSPP Distance Estimates

We next consider how systematic errors in the determination of distance could affect our result. In our analysis, we select stars with distances in the range $0.84 \text{ kpc} < d < 1.64 \text{ kpc}$. If the distances to K dwarfs are over-estimated by the SSPP, then more K-type dwarfs in our sample are expected to reside closer to the Galactic disk plane, and the fraction of K-type dwarfs that belong to the thick disk is over-estimated in our sample. In this case, we unintentionally compare the low- $|z|$ K dwarfs and high- $|z|$ G-type dwarfs, leading to a higher value of $\langle V_\phi \rangle_{\text{med}}$ for K-type dwarfs at a fixed $[\text{Fe}/\text{H}]$. In order to test this bias, we construct two different samples of K-type dwarfs selected by the same criteria as in Section 2, but assigned distances that are 20% smaller or larger compared to the adopted distance. In both instances, we confirm that the difference between the resultant $\langle V_\phi \rangle_{\text{med}} - [\text{Fe}/\text{H}]$ relation and the original one is less than 20 km s^{-1} at $[\text{Fe}/\text{H}] > -1.5$. We conclude that a systematic error of $\sim 20\%$ in distance determination cannot explain the observed difference in the $\langle V_\phi \rangle_{\text{med}} - [\text{Fe}/\text{H}]$ relationship between the G- and K-type dwarfs.

4.2.4. Mock Data Analysis

In order to check the validity of our results, we also examine how random and/or systematic errors in the observed quantities (such as distance and metallicity) could affect our results in Figures 1 and 2. For this purpose, we construct a set of realistic mock catalogs in which the information on effective temperature, surface gravity, metallicity, distance, Galactic latitude and longitude is identical to that of our real sample,¹⁰ but the information on line-of-sight velocity and proper motion reflects a given distribution function model as well as assumed realistic errors in metallicity, distance, line-of-sight velocity and proper motion. Note that the effect of metal accretion is not taken into account in our mock catalogs. (See Appendix for the full description of our mock catalogs.)

We consider various models of random and/or systematic errors in the observed quantities, and prepare 100 mock catalogs for each error model. Then we perform

¹⁰ Since the values of T_{eff} , $\log g$, $[\text{Fe}/\text{H}]$, and d are the same as those of the real sample, the spatial and metallicity distributions of G- and K-type dwarfs of any given mock catalog are identical to those of our real sample.

the same analyses on our mock catalogs as applied to our real sample, and derive the $\langle V_\phi \rangle_{\text{med}}\text{--}[\text{Fe}/\text{H}]$ relations which correspond to Figures 1 (full sample) and 2 (z_{max} -limited subsamples).

First, we find that the $\langle V_\phi \rangle_{\text{med}}\text{--}[\text{Fe}/\text{H}]$ relations for G- and K-type dwarfs in our mock catalogs are statistically identical, if we do not introduce any spectral-type dependence in the observational errors. Noting that the spatial distributions of the mock G- and K-type dwarfs are identical to those of the real G- and K-type dwarfs, this result justifies our starting point that the spatial distributions of our G- and K-type dwarfs are essentially identical (section 2.3).

Secondly, we find that the offset in the $\langle V_\phi \rangle_{\text{med}}\text{--}[\text{Fe}/\text{H}]$ relation similar to that in Figure 1 is seen only when the random or systematic errors in $[\text{Fe}/\text{H}]$ depend on the spectral type. In addition, we find that when such an offset is seen in the full sample, a similar offset is also seen in the low- z_{max} subsample, and vice versa. In other words, random or systematic errors in $[\text{Fe}/\text{H}]$ either produce an offset for *both* Figures 1(c) and 2(a), or produce no offset for *both* of these figures. This finding is in sharp contrast with our results for the real sample, in which a clear offset is seen only in Figure 1(c) and not in Figure 2(a). Moreover, we also find that the offset in the $\langle V_\phi \rangle_{\text{med}}\text{--}[\text{Fe}/\text{H}]$ relation for the high- z_{max} subsample is, if anything, less clear than that for the low- z_{max} subsample. Presumably, this result is due to the smaller number of stars in the high- z_{max} subsample. This finding is also opposite to our results for the real sample, in which a clearer offset is seen in Figure 2(b) than in Figures 2(a).

These results suggest that the observed offset in the $\langle V_\phi \rangle_{\text{med}}\text{--}[\text{Fe}/\text{H}]$ relation cannot be explained by observational errors that may or may not depend on the spectral type. Therefore, we conclude that the observed offset in Figures 1 and 2(b), as well as apparent non-existence of the offset in Figure 2(a), are all real.

5. DISCUSSION

In this paper we have derived the relation of $\langle V_\phi \rangle_{\text{med}}$ (median value of V_ϕ) as a function of $[\text{Fe}/\text{H}]$ for halo G- and K-type dwarfs from SDSS DR8. We find that the run of $\langle V_\phi \rangle_{\text{med}}$ vs. $[\text{Fe}/\text{H}]$ can be characterized by a boundary metallicity, $[\text{Fe}/\text{H}]_{\text{knee}}$, below which the nearly non-rotating halo stars dominate, and that $[\text{Fe}/\text{H}]_{\text{knee}}$ for G-type dwarfs occurs at a higher abundance than that for K-type dwarfs by an offset of $\delta \simeq 0.20$ dex. This offset is also seen for those sample stars that have large vertical motion. Below we consider the implications of this result.

5.1. Evidence of Metal Accretion onto Main-Sequence Halo Stars

We interpret this non-zero value of $\delta \simeq 0.20$ dex between the characteristic metallicities of halo G- and K-type dwarfs to be the first tentative evidence that halo stars have been *externally* polluted by the accretion of metal-enriched gas from their natal clouds. The effect is more noticeable for G-type dwarfs, whose convective envelopes are shallower than those of K-type dwarfs, since they will not have diluted accreted material as fully.

If this interpretation is correct, we expect an even larger offset in metallicity for red giants (e.g., K giants), which possess deeper surface convective envelopes than

K-type dwarfs (Yoshii 1981). That is, the knee of the $\langle V_\phi \rangle_{\text{med}}\text{--}[\text{Fe}/\text{H}]$ relation for K giants, if plotted as in Figure 1, should be located to the left of that for K dwarfs. Although there is no large publicly available database of nearby K giants, other types of post-main-sequence stars might serve as alternatives, since the surface heavy element abundance is expected to remain unchanged when red giants evolve into either horizontal-branch stars or RR Lyrae stars. During the course of this evolution, red giants lose mass from their surface convective envelopes. The total amount of mass loss is expected to be $\simeq 0.2 M_\odot$ for a red giant of initially $0.8 M_\odot$ (see Yoshii 1981, and references therein), which is smaller than the total mass of the surface convective envelope ($\simeq 0.3 M_\odot$) in the red-giant stage (Sweigart & Gross 1978).

Thus, instead of red giants, we have explored the $\langle V_\phi \rangle_{\text{med}}\text{--}[\text{Fe}/\text{H}]$ relation for 290 blue horizontal-branch (BHB) stars with $T_{\text{eff}} > 7500$ K, $\log g < 3.8$, located at $2 \text{ kpc} < |z| < 5 \text{ kpc}$, $5 \text{ kpc} < R < 20 \text{ kpc}$, taken from Xue et al. (2011). Here, R and $|z|$ are the Galactocentric distance projected onto the Galactic disk plane and the distance above or below the disk plane, respectively. The cuts in T_{eff} and $\log g$ are adopted following the selection criteria proposed by R. Santucci et al. (in preparation).

In Figure 3, we show the distribution of BHB stars in the $V_\phi\text{--}[\text{Fe}/\text{H}]$ space, along with the median value $\langle V_\phi \rangle_{\text{med}}$ for the binned sample. From inspection of this figure, the $\langle V_\phi \rangle_{\text{med}}$ of BHB stars is nearly constant (consistent with 0 km s^{-1}) at $[\text{Fe}/\text{H}] < [\text{Fe}/\text{H}]_{\text{knee}} \simeq -1.7$.¹¹ This suggests that inner-halo BHB stars dominate over metal-weak thick-disk BHB stars below $[\text{Fe}/\text{H}] = [\text{Fe}/\text{H}]_{\text{knee}}$ at $2 \text{ kpc} < |z| < 5 \text{ kpc}$. Noting that a lower value of $[\text{Fe}/\text{H}]_{\text{knee}}$ is expected for a sample of stars with lower $|z|$ (due to the larger fraction of thick-disk stars in the sample), we expect that $[\text{Fe}/\text{H}]_{\text{knee}}$ for BHB stars would be even lower than -1.7 if we could obtain a BHB sample with distances in the range $0.84 \text{ kpc} < d < 1.64 \text{ kpc}$, as was used above for the G- and K-dwarf samples. Since the positions of $[\text{Fe}/\text{H}]_{\text{knee}}$ for the G and K-type dwarfs are -1.4 and -1.6 , respectively, in this distance range (see Figure 1), it follows that $[\text{Fe}/\text{H}]_{\text{knee}}$ for BHB stars should be lower, by *at least* 0.3 dex and 0.1 dex, respectively, if these samples could be fairly compared. This may indicate that the BHB stars are even less affected by surface metal pollution than K-type dwarfs. The sample of 290 BHB stars is not sufficiently large to be certain of this effect, but the present result does serve to support the accretion hypothesis for halo stars. Surveys such as LAMOST and Gaia will provide larger kinematically unbiased samples of low-mass dwarfs and red giants. At that stage, we will be able to compare the chemo-dynamical correlations of these stars more rigorously, and test the metal accretion hypothesis thoroughly.

5.2. Where did the Metal Accretion Take Place?

¹¹ The plateau value of $\langle V_\phi \rangle_{\text{med}}$ at $[\text{Fe}/\text{H}] < [\text{Fe}/\text{H}]_{\text{knee}}$ for the BHB sample ($\simeq 0 \text{ km s}^{-1}$) is lower than that for G/K-type dwarfs ($\simeq 50 \text{ km s}^{-1}$; see Figure 1). This discrepancy seems to arise from the different spatial regions covered by these samples. In fact, Chiba & Beers (2000) find that the mean rotational velocity (V_ϕ) for nearby metal-poor stars with $[\text{Fe}/\text{H}] < -1.5$ is higher for those sample stars with smaller $|z|$ [see their Figure 3(a)], which is consistent with our discrepancy.

As mentioned in the Introduction, the efficiency of metal accretion in halo stars is proportional to v_{rel}^{-3} , where v_{rel} is the relative velocity of the star and the colliding gas. Therefore, metal accretion onto halo stars may or may not be important, depending on the nature of the environments in which it could take place. Recent observations (Carollo et al. 2007, 2010; Beers et al. 2012) and numerical simulations (Font et al. 2011; McCarthy et al. 2012; Tissera et al. 2013) suggest that the stellar halo of the Milky Way comprises two distinct components with different origins, which are often referred to as the inner- and outer-halo populations. In this picture, inner-halo stars formed from relatively more massive sub-galactic systems ($10^9\text{--}10^{10} M_{\odot}$) in the main progenitors of the Milky Way, while much smaller sub-galactic systems ($10^7\text{--}8 M_{\odot}$ or less), similar to lower-mass dwarf-like galaxies, were disrupted to contribute the bulk of the low-metallicity outer-halo stars. In the progenitor systems of the inner-halo stars, the internal velocity dispersion is expected to be $\sim 30 \text{ km s}^{-1}$ (Tissera et al. 2013), so that the above-mentioned v_{rel} may have been too large for inner-halo stars to experience efficient metal accretion. On the other hand, the internal velocity dispersion of ultra-faint dwarf galaxies – whose constituent stars are typically as metal-poor as $[\text{Fe}/\text{H}] \lesssim -2.0$, similar to nearby outer-halo stars – is $\sim 5 \text{ km s}^{-1}$ (Simon & Geha 2007; Walker et al. 2009; see also Yoshii & Arimoto 1987), so that v_{rel} may have been small enough to enable efficient metal accretion onto constituent stars. Therefore, in this inner/outer halo picture, the outer-halo stars are much more likely to have experienced metal accretion. In other words, if the dual halo picture is correct, we expect that inner-halo dominated sample of G- and K-type dwarfs would exhibit little or no offset in the $\langle V_{\phi} \rangle_{\text{med}}\text{--}[\text{Fe}/\text{H}]$ relation, while the outer-halo dominated sample of G- and K-type dwarfs would show noticeable offsets.

Observationally, it is suggested that the fraction of outer-halo stars increases as z_{max} increases (Carollo et al. 2010). Thus, if we divide each of our G- and K-dwarf samples into two subsamples with respect to z_{max} , the fraction of outer-halo stars is expected to be larger in the higher- z_{max} subsample than in the lower- z_{max} one. It follows that we expect a clearer offset in the $\langle V_{\phi} \rangle_{\text{med}}\text{--}[\text{Fe}/\text{H}]$ relation for the higher- z_{max} subsample. This expectation is indeed consistent with the results in Figure 2, in which we observe a clearer offset in the $\langle V_{\phi} \rangle_{\text{med}}\text{--}[\text{Fe}/\text{H}]$ relation for our sample stars with $z_{\text{max}} > 3 \text{ kpc}$, and not for those stars with $z_{\text{max}} < 3 \text{ kpc}$.¹² These results can be understood if a dual inner/outer halo applies to the Milky Way, as originally suggested by Carollo et al. (2007), and metal accretion is efficient only for stars associated with the progenitors of the outer halo.

We note here that typical halo stars with $z_{\text{max}} > 3 \text{ kpc}$ would penetrate through the Galactic disk with a velocity of $v_{\text{rel}} > 100 \text{ km s}^{-1}$ relative to the gas clouds in the disk. Therefore, metal accretion when the halo stars pen-

etrate the Galactic disk plane accounts for only a negligible fraction of the total amount of metals accreted onto halo stars, supporting the view of Frebel et al. (2009). However, the fact that we see a clear offset in panel (b) of Figure 3 suggests that the outer-halo stars are likely to have experienced metal accretion within their progenitor systems, which were *later* disrupted.

5.3. Impact on the Metallicity Distribution Function in the Stellar Halo System

One obvious impact of our results is that the metallicity distribution function (MDF) of halo main-sequence stars may need to be re-examined. In the hierarchical galaxy formation scenario, halo stars form in sub-galactic systems that are later disrupted by tidal interaction with the Galaxy, hence halo stars originating from these disrupted systems are likely to have experienced metal accretion within these systems (Shigeeyama et al. 2003; Suda et al. 2004; Komiya et al. 2010). As a consequence, the shape of the MDF of halo stars is expected to be skewed toward higher $[\text{Fe}/\text{H}]$ when compared to their original MDF, because the surface metallicity is enhanced for stars with lower $[\text{Fe}/\text{H}]$ due to their shallow surface convective envelopes, while it is less enhanced for stars with higher $[\text{Fe}/\text{H}]$ due to their deeper surface convective envelopes (Mengel et al. 1979).

In this respect, it is intriguing to note the apparent discrepancy between the MDFs of main-sequence turn-off (MSTO) stars and BHB stars in the outer halo region of the Milky Way. Sesar et al. (2011) show that the median metallicity of MSTO stars at Galactocentric distances in the range of $10 \text{ kpc} < r < 30 \text{ kpc}$ is $[\text{Fe}/\text{H}] \simeq -1.5$, almost independent of r .¹³ On the other hand, Beers et al. (2012) show that the median metallicity of BHB stars at $10 \text{ kpc} < r < 40 \text{ kpc}$ is $[\text{Fe}/\text{H}] \simeq -2.0$, almost independent of r .¹⁴ This discrepancy can be well explained by the accretion hypothesis. MSTO and BHB stars are of similar age, yielding no systematic difference in the mass accreted in their main-sequence stage. Thus, the surface metallicity of BHB stars is much less enhanced than that of MSTO stars, because the red giants that were progenitors of the stars presently on the BHB had very deep surface convective envelopes compared to MSTO stars (see section 5.1).

Furthermore, noting that the surface convective envelopes of MSTO stars are shallower than those of G-type dwarfs, it is also interesting to note that the apparent offset in the median metallicity of the MDF for MSTO and BHB stars ($[\text{Fe}/\text{H}]_{\text{median,MSTO}} - [\text{Fe}/\text{H}]_{\text{median,BHB}} \simeq 0.5 \text{ dex}$) is consistent with the offset in the break metallicity ($[\text{Fe}/\text{H}]_{\text{knee,G}} - [\text{Fe}/\text{H}]_{\text{knee,BHB}} \gtrsim 0.3 \text{ dex}$) of the $\langle V_{\phi} \rangle_{\text{med}}\text{--}[\text{Fe}/\text{H}]$ relation for G-type dwarfs and BHB stars (see section 5.1). Our interpretation of this consistency in terms of the accretion hypothesis may be tested based on a much larger sample of BHB stars or red giants that should be available in the near future.

Another intriguing aspect of the observed halo MDF is the possible existence of a cutoff metallicity at

¹² Our boundary at $z_{\text{max}} = 3 \text{ kpc}$ is smaller than that adopted in Carollo et al. (2010), so that we have a sufficient number of stars in the higher- z_{max} subsample. However, this difference is not crucially important, since our aim is to examine two subsamples with different fractions of inner/outer-halo stars. Our higher- z_{max} subsample includes numerous stars with z_{max} as large as 10–50 kpc.

¹³ See panels W3 and W4 in Figure 12 of Sesar et al. (2011), in which the influence from known substructures in the halo is not significant.

¹⁴ See the right-hand panels in Figure 15 of Beers et al. (2012), in which the contamination from the Sagittarius dwarf galaxy is minimized, and Figure 4 of Carollo et al. (2007).

$[\text{Fe}/\text{H}]_{\text{cutoff}} \simeq -4$, below which the MDF shows a sharp decline (Schörck et al. 2009; Li et al. 2010; see also Yong et al. 2013). There are not yet a sufficient number of stars known with $[\text{Fe}/\text{H}] < -3.5$, let alone with $[\text{Fe}/\text{H}] < -4.0$, to evaluate whether the cutoff is real, or simply the result of small number statistics in the ultra metal-poor regime. Future observations of G/K-type dwarfs might well detect a spectral-type dependence of this cutoff metallicity, in the sense that $[\text{Fe}/\text{H}]_{\text{cutoff,K}} < [\text{Fe}/\text{H}]_{\text{cutoff,G}}$, if metal accretion and subsequent surface metal enhancement does indeed take place among metal-poor halo stars.

5.4. On the Case of ω Centauri

Some globular clusters appear to be ideal places to test the metal accretion hypothesis, if they are regarded as closed systems and the constituent stars are coeval, or nearly so. Stanford et al. (2007) investigate the metallicities of stars in the globular cluster ω Cen, and find that the peak metallicity of near-turn-off stars is systematically higher than that of red giant branch (RGB) stars, by 0.01-0.05 dex (see their Figure 2). This offset is smaller than the uncertainty in the derived $[\text{Fe}/\text{H}]$ for their sample (0.15-0.20 dex). However, taking into account that the surface convective envelope is deeper for RGB stars than near-turn-off stars, the sense of the reported gap is in agreement with the prediction from the metal accretion hypothesis.

If the reported gap (0.01-0.05 dex) between near-turn-off stars and RGB stars is due to metal accretion, we expect that the typical metallicities of G- and K-type dwarfs in ω Cen are different from each other by less than 0.05 dex, because of the milder difference in the depth of surface convective envelope between G- and K-type dwarfs. If we take into account the observed offset of $\simeq 0.20$ dex in Figure 2(b), the metal accretion in typical progenitor systems of the Milky Way outer halo is more significant than that in ω Cen. Noting that the efficiency of metal accretion is proportional to v_{rel}^{-3} , the seemingly low efficiency within ω Cen indicates that typical progenitor systems of the outer halo must have smaller internal velocity dispersions than that of ω Cen. It is suggested that such progenitor systems are similar to the currently observed ultra-faint dwarf galaxies (with central velocity dispersion $\sim 5 \text{ km s}^{-1}$), and that the contribution from large and compact globular clusters (such as ω Cen, with central velocity dispersion $\simeq 17 \text{ km s}^{-1}$; Sollima et al. 2009) to the outer halo is not significant.

5.5. Implication for the First Stars

If primordial (zero-metal) stars from the very first generation (with main-sequence masses below $0.8M_{\odot}$) were able to form, they could survive until today, and possibly be observed. Here we consider this possibility from the perspective of the accretion hypothesis.

The mass range of the first stars has been long debated, but some nucleosynthesis constraints have recently been placed by the discovery of four hyper metal-poor (HMP; technically, Fe-poor) stars with $[\text{Fe}/\text{H}] \lesssim -5$ (HE 01072-5240: Christlieb et al. 2002; HE 1327-2326: Frebel et al. 2005; HE 0557-4840: Norris et al. 2007; SDSS J102915+172927: Caffau et al. 2012). Three of the four stars (excluding SDSS J102915+172927) ex-

hibit elemental abundance patterns that are significantly enhanced with carbon (C) and nitrogen (N), and can be well-explained if they are second-generation stars, formed out of an interstellar medium that was chemically enriched by supernova ejecta from $25M_{\odot}$ primordial stars (Umeda & Nomoto 2003; Iwamoto et al. 2005; Nomoto et al. 2013).

However, if we allow for the metal accretion hypothesis, as suggested to apply in this paper, it is possible to regard the above-mentioned HMP stars as surviving primordial stars whose surfaces were polluted by the accretion of the supernova ejecta of $25M_{\odot}$ primordial stars (Shigeyama et al. 2003). Since the mass of these stars is as small as $0.8M_{\odot}$, our interpretation has an implicit requirement for the mass of primordial stars to range from less than $1M_{\odot}$ up to more than a few tens of M_{\odot} , as predicted by some authors (Yoshii & Saio 1986; Nakamura & Umemura 2001). In this respect, it is worth mentioning that SDSS J102915+172927 is an $0.7M_{\odot}$ star with no significant C and N enhancement. The mass fraction of heavy elements derived for this star, $Z < 7.4 \times 10^{-7}$, is the lowest known to date, and heavy-element cooling in metal-poor gas with $Z < Z_{\text{crit}} = 10^{-5} - 10^{-6}$ is superseded by purely atomic or molecular hydrogen or zero-metal cooling (Silk 1977; Yoshii & Sabano 1980; Bromm et al. 2001; Smith et al. 2009; Safranek-Shrader et al. 2010). Therefore, the discovery of a $0.7M_{\odot}$ star with $Z < Z_{\text{crit}}$ indicates that this star could indeed have formed by zero-metal cooling. In other words, the zero-metal cooling process turns out to be able to produce primordial stars with the masses below $1M_{\odot}$.

We propose that at least some of the HMP stars could be surviving primordial stars that have experienced surface metal pollution after they formed. Given that the environments in which such pollution can occur is limited, we expect that even more HMP metal-poor stars similar to SDSS J102915+172927, with $Z \ll Z_{\text{crit}}$, may well be discovered.

6. SUMMARY

In this paper we have described possible observational evidence for the surface metal pollution of halo stars due to the accretion of metal-enriched material onto stellar surfaces, as theoretically predicted by Yoshii (1981). If we take at face value our analysis of an additional sample of BHB stars, it might be the case that the initial metallicities of halo G-type dwarfs and halo K-type dwarfs are at least ~ 0.3 dex and ~ 0.1 dex *lower* than their observed atmospheric metallicities, respectively. We also suggest this interpretation, along with extant observations of HMP stars, may provide confirmation that the lower mass limit of the primordial initial stellar mass function extends to below $1M_{\odot}$.

In our current analysis, we could only compare the $\langle V_{\phi} \rangle_{\text{med}} - [\text{Fe}/\text{H}]$ correlation for different types of stars, due to the large extant errors in proper motion. However, the situation will be greatly improved in the near future, when the Gaia satellite and large ground-based telescopes provide truly enormous samples of disk and halo stars with much more accurate kinematic and chemical information. Such datasets will enable analyses of other chemo-dynamical correlations – e.g., correlations between the full velocity dispersion tensors and surface

metal abundances – as well as more rigorous analyses of the $\langle V_\phi \rangle_{\text{med}}\text{--}[\text{Fe}/\text{H}]$ relation.

We thank the referee for critical but constructive comments on our manuscript. KH thanks Takafumi Sono, Masaomi Tanaka, Takuma Suda, and Akimasa Kataoka for stimulating discussions. KH is supported by JSPS Research Fellowship for Young Scientists (23.954). YY

acknowledges partial support from the Grant-in-Aids of Scientific Research (17104002) of the Ministry of Education, Science, Culture and Sports of Japan. TCB acknowledges partial support for this work from grant PHY 08-22648: Physics Frontiers Center / JINA, awarded by the US National Science Foundation. YSL is a Tombaugh Fellow.

APPENDIX

MOCK CATALOGS OF G/K-TYPE DWARFS

Construction of Mock Catalogs

In section 4.2.4, we used a set of mock catalogs of G/K-type dwarfs in order to investigate the reality of the observed offset in the $\langle V_\phi \rangle_{\text{med}}\text{--}[\text{Fe}/\text{H}]$. Here we present some additional information on these mock catalogs.

The observed (real) catalog of G/K-type dwarfs can be mathematically expressed as

$$\{ (T_{\text{eff},i}, \log g_i, [\text{Fe}/\text{H}]_i, d_i, \ell_i, b_i, v_{\text{los},i}^{\text{hel}}, PM_i^\ell, PM_i^b) \mid i = 1, \dots, N \}, \quad (\text{observed sample}), \quad (\text{A1})$$

where N is the total number of G/K-type dwarfs and the nine quantities for the i -th entry denote the effective temperature ($T_{\text{eff},i}$), surface gravity ($\log g_i$), atmospheric metallicity ($[\text{Fe}/\text{H}]_i$), SSPP distance (d_i), Galactic longitude (ℓ_i), Galactic latitude (b_i), heliocentric line-of-sight velocity ($v_{\text{los},i}^{\text{hel}}$), proper motion in the ℓ - and b -directions (PM_i^ℓ , PM_i^b) of the i -th star. We generate each of our mock catalogs so that the i -th star in the mock catalog ($i = 1, \dots, N$) has the same information on effective temperature, surface gravity, metallicity and 3-D position as those of the i -th star in our real (observed) catalog, while its 3-D velocity is assigned according to a given realistic Galactic model, as well as to the assumed error models. Namely, the j -th mock catalog ($j = 1, \dots, M$) can be expressed as

$$\left\{ (T_{\text{eff},i}, \log g_i, [\text{Fe}/\text{H}]_i, d_i, \ell_i, b_i, v_{\text{los},i,j}^{\text{mock-obs,hel}}, PM_{i,j}^{\text{mock-obs},\ell}, PM_{i,j}^{\text{mock-obs},b}) \mid i = 1, \dots, N \right\}, \quad (j\text{-th mock catalog}). \quad (\text{A2})$$

In assigning the 3-D velocity information to the i -th star of a given mock catalog, we follow four steps:

- **Step 1** Assign the ‘true’ $[\text{Fe}/\text{H}]$ and the ‘true’ 3-D position to the mock star;
- **Step 2** Determine whether the i -th mock star belongs to halo or thick disk with a certain probability based on the ‘true’ $[\text{Fe}/\text{H}]$ and the ‘true’ 3-D position;
- **Step 3** Assign the ‘true’ 3-D velocity according to the distribution function model of the halo and thick disk;
- **Step 4** Decompose the ‘true’ 3-D velocity into the line-of-sight velocity and proper motion and add realistic observational errors.

Note that the ‘true’ $[\text{Fe}/\text{H}]$ and the ‘true’ distance are only used as internal variables, and do not appear explicitly in the mock catalogs. In the following, we describe each step in more detail.

In **Step 1**, we assign the ‘true’ metallicity

$$[\text{Fe}/\text{H}]_{i,j}^{\text{true}} = [\text{Fe}/\text{H}]_i + E_r([\text{Fe}/\text{H}]_i) \quad (\text{A3})$$

to the i -th star in the j -th mock catalog. Here, E_r is the error-correcting term. Also, we assign the ‘true’ distance

$$d_{i,j}^{\text{true}} = d_i \times \mathcal{N}(\mu_{\text{dist}}, 0.2) \quad (\text{A4})$$

to the i -th star. Here, $\mathcal{N}(\mu, \sigma)$ is a random number generator that generate random numbers obeying a Gaussian distribution function with the mean of μ and the dispersion of σ . When there is no systematic error, we set $\mu_{\text{dist}} = 1$. The choice of $\sigma = 0.2$ is motivated by the $\sim 20\%$ random error in the distance estimation. We note that there is a tiny probability for the random number generator \mathcal{N} to generate negative numbers. In that case, we set $d_{i,j}^{\text{true}} = 0.1$ kpc.

In **Step 2**, we randomly assign a flag of H (halo) or TD (thick disk) to the i -th star with a probability of p or $(1 - p)$, respectively, where p is defined by

$$p = \frac{f_H([\text{Fe}/\text{H}]_{i,j}^{\text{true}})}{f_H([\text{Fe}/\text{H}]_{i,j}^{\text{true}}) + f_{TD}([\text{Fe}/\text{H}]_{i,j}^{\text{true}}) \times D(d_{i,j}^{\text{true}} \cdot \sin b_i)}. \quad (\text{A5})$$

Here, $D(z)$ describes the density profile of the thick disk as a function of the vertical distance from the Galactic disk plane $|z|$; and f_H and f_{TD} denote the MDFs at the Galactic plane ($z = 0$ kpc) of halo and thick disk stars, respectively.

We assume the following models for these functions:

$$f_k([\text{Fe}/\text{H}]) = F_k \times \frac{1}{\sqrt{2\pi}\sigma_k} \exp \left[-\frac{1}{2} \left(\frac{[\text{Fe}/\text{H}] - \mu_k}{\sigma_k} \right)^2 \right], \quad (k = H, TD), \quad (\text{A6})$$

$$D(z) = \exp \left[-\frac{|z|}{h_z} \right], \quad h_z = 1.0 \text{ kpc}, \quad (\text{A7})$$

and we set $(F_H, \mu_H, \sigma_H) = (0.001, -1.5, 0.3)$, $(F_{TD}, \mu_{TD}, \sigma_{TD}) = (0.040, -0.6, 0.2)$. We note here that we do not expect significant contribution from the thin disk, because of our metallicity cut of $[\text{Fe}/\text{H}] < -0.5$.

In **Step 3**, we assign the ‘true’ 3-D velocity of the i -th star in the usual Galactic cylindrical coordinate system by

$$(V_{R,i,j}^{true}, V_{\phi,i,j}^{true}, V_{z,i,j}^{true}) = \begin{cases} (\mathcal{N}(0, 80), \mathcal{N}(50, 150), \mathcal{N}(0, 70)) \text{ km s}^{-1} & (flag = H), \\ (\mathcal{N}(0, 30), \mathcal{N}(180, 30), \mathcal{N}(0, 30)) \text{ km s}^{-1} & (flag = TD). \end{cases} \quad (\text{A8})$$

Here, it is assumed that the mean rotational velocities of halo and thick disk are 50 km s^{-1} and 180 km s^{-1} , respectively.

In **Step 4**, we calculate the ‘true’ heliocentric line-of-sight velocity $v_{los,i,j}^{true,hel}$ and the ‘true’ proper motion $PM_{i,j}^{true,\ell}$, $PM_{i,j}^{true,b}$ of the i -th mock star in j -th mock catalog, by using the ‘true’ distance $d_{i,j}^{true}$ and by assuming the same LSR and peculiar solar velocity as those described in section 3.1. Then we calculate the ‘mock-observed’ values for these quantities by using

$$v_{los,i,j}^{mock-obs,hel} = v_{los,i,j}^{true,hel} + \mathcal{N}(0, 2) \text{ km s}^{-1}, \quad (\text{A9})$$

$$PM_{i,j}^{mock-obs,\ell} = PM_{i,j}^{true,\ell} + \mathcal{N}(0, 3.5) \text{ mas yr}^{-1}, \quad (\text{A10})$$

$$PM_{i,j}^{mock-obs,b} = PM_{i,j}^{true,b} + \mathcal{N}(0, 3.5) \text{ mas yr}^{-1}. \quad (\text{A11})$$

We note that the adopted errors in the line-of-sight velocity (2 km s^{-1}) and in proper motion (3.5 mas yr^{-1}) are typical values in our real sample.

TABLE 1
METALLICITY ERROR MODELS IN THE MOCK CATALOGS

Model	$E_r([\text{Fe}/\text{H}])$ for G-type dwarfs	$E_r([\text{Fe}/\text{H}])$ for K-type dwarfs
Model A	$\mathcal{N}(0, 0.2)$	$\mathcal{N}(0, 0.2)$
Model B	$\mathcal{N}(0, 0.2)$	$\mathcal{N}(0, 0.3)$
Model C	$\begin{cases} \mathcal{N}(0, 0.2) & ([\text{Fe}/\text{H}] \geq -1) \\ \mathcal{N}(0, 0.2) + 0.2 \times ([\text{Fe}/\text{H}] + 1.0) & ([\text{Fe}/\text{H}] < -1) \end{cases}$	$\begin{cases} \mathcal{N}(0, 0.2) & ([\text{Fe}/\text{H}] \geq -1) \\ \mathcal{N}(0, 0.2) - 0.2 \times ([\text{Fe}/\text{H}] + 1.0) & ([\text{Fe}/\text{H}] < -1) \end{cases}$

Mock Observations of Mock Catalogs

Observational errors in $[\text{Fe}/\text{H}]$ and distance are the most important factors that affect the derived $\langle V_\phi \rangle_{\text{med}} - [\text{Fe}/\text{H}]$ relations. In order to evaluate how observational errors in $[\text{Fe}/\text{H}]$ affect our analyses, we consider three models of the error-correcting term $E_r([\text{Fe}/\text{H}])$, as presented in Table 1. Among these models, Model A does not carry a spectral-type dependence in the $[\text{Fe}/\text{H}]$ error, while Models B and C are designed to carry this spectral-type dependence. We also consider three types of systematic errors in distance, by adopting $\mu_{dist} = 0.8, 1.0$, or 1.2 . For each of the nine combinations of the error models (three for the $[\text{Fe}/\text{H}]$ error and three for the distance error), we generate 100 mock catalogs and derive the $\langle V_\phi \rangle_{\text{med}} - [\text{Fe}/\text{H}]$ relations.

In Figures 4, 5, and 6, we show the results for Models A, B, and C, respectively, with μ_{dist} fixed to be 1.0. In these figures, we show the median curve of 100 $\langle V_\phi \rangle_{\text{med}} - [\text{Fe}/\text{H}]$ relations derived from the mock catalogs. The panels (a), (b), and (c) correspond to Figures 1(c), 2(a), and 2(b), respectively.

Figure 4 suggests that, if the observational errors in $[\text{Fe}/\text{H}]$ do not possess a spectral-type dependence (Model A), the resultant $\langle V_\phi \rangle_{\text{med}} - [\text{Fe}/\text{H}]$ relations are statistically identical for G- and K-type dwarfs. On the other hand, Figures 5 and 6 suggest that we expect an offset in the $\langle V_\phi \rangle_{\text{med}} - [\text{Fe}/\text{H}]$ relation for the full sample and the low- z_{max} subsample, if there is a spectral-type dependence in the observational errors in $[\text{Fe}/\text{H}]$ (Model B or C), although the offset is not very clear for the high- z_{max} subsample (due to the small sample size).

By comparing the panels (a) and (b) in Figures 4, 5, and 6, it is suggested that, whenever we see an offset in the full sample [panel (a)], we should also see a similar offset in the low- z_{max} subsample [panel (b)]. In other words, if the observed offset in Figure 1(c) is due to the observational errors in $[\text{Fe}/\text{H}]$, then a similar offset is also expected in Figure 2(a) as well. Thus, it seems that the detected offset in Figures 1(c) and 2(b), as well as the non-existence of the offset in Figure 2(a), are due to neither an observational error in $[\text{Fe}/\text{H}]$ nor its spectral-type dependence.

If we further vary the value of μ_{dist} for G- and/or K-type dwarfs, the results are essentially the same as in the case of $\mu_{dist} = 1.0$. The only difference is in the overall location of the $\langle V_\phi \rangle_{\text{med}} - [\text{Fe}/\text{H}]$ curves. If μ_{dist} is set to be 0.8 and the

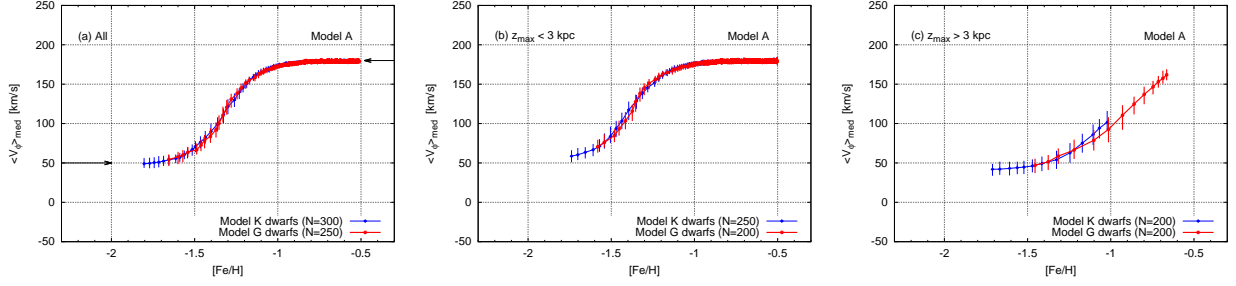


FIG. 4.— The $\langle V_\phi \rangle_{\text{med}}\text{--}[\text{Fe}/\text{H}]$ relations for 100 mock catalogs with $\mu_{\text{dist}} = 1.0$. The implemented error in $[\text{Fe}/\text{H}]$ is described by Model A for these mock catalogs. The red and blue lines indicate the median curve of 100 $\langle V_\phi \rangle_{\text{med}}\text{--}[\text{Fe}/\text{H}]$ relations for G- and K-type dwarfs, respectively. (a) The result for the full sample without z_{max} cut applied, which corresponds to Figure 1(c). The horizontal arrows at 50 km s^{-1} and 180 km s^{-1} indicate the mean velocities of halo and thick-disk stars, respectively, expected from the input distribution function model [see equation (A8)]. (b) The result for the subsample of stars with $z_{\text{max}} < 3 \text{ kpc}$, which corresponds to Figure 2(a). (c) The result for the subsample of stars with $z_{\text{max}} > 3 \text{ kpc}$, which corresponds to Figure 2(b).

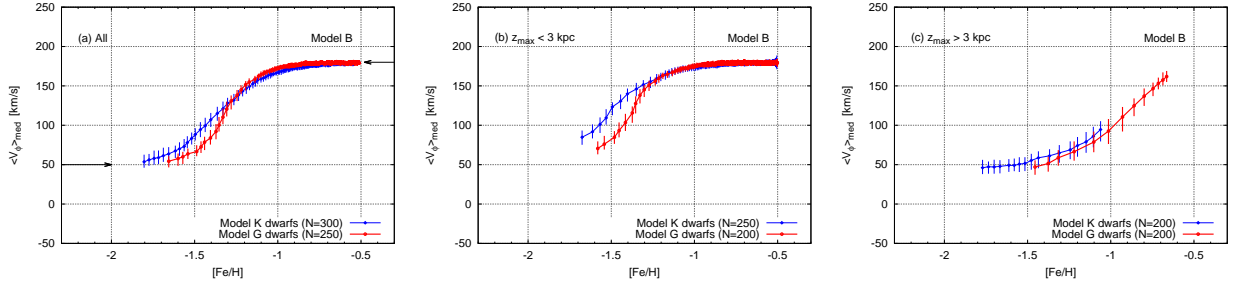


FIG. 5.— The same as in Figure 4, but for 100 mock catalogs in which the error in $[\text{Fe}/\text{H}]$ is described by Model B.

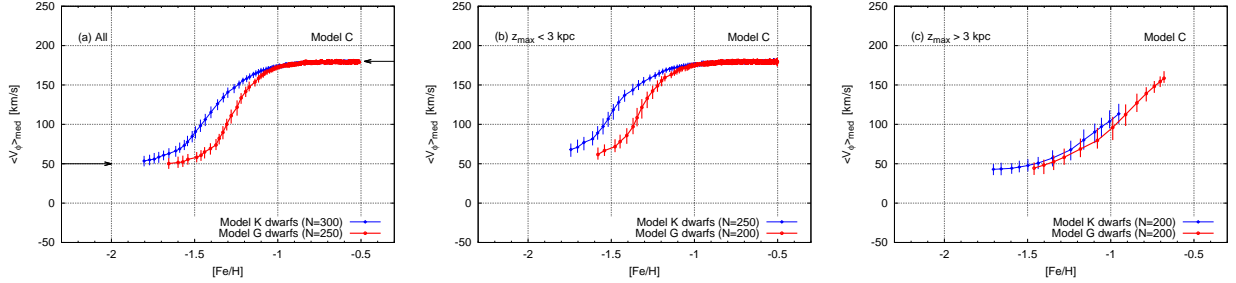


FIG. 6.— The same as in Figure 4, but for 100 mock catalogs in which the error in $[\text{Fe}/\text{H}]$ is described by Model C.

SSPP distance is overestimated, the resultant curve of the $\langle V_\phi \rangle_{\text{med}}\text{--}[\text{Fe}/\text{H}]$ relation is shifted downwards (toward lower $\langle V_\phi \rangle_{\text{med}}$), due to the overestimate of the relative velocities of the sample stars with respect to the Sun. On the other hand, if μ_{dist} is set to be 1.2 and the SSPP distance is underestimated, the resultant curve of $\langle V_\phi \rangle_{\text{med}}\text{--}[\text{Fe}/\text{H}]$ relation is shifted upwards. The effect of μ_{dist} is most prominently seen at the low-metallicity tail of the $\langle V_\phi \rangle_{\text{med}}\text{--}[\text{Fe}/\text{H}]$ relation. For example, if we adopt Model A, the plateau value of $\langle V_\phi \rangle_{\text{med}}$ in the low-metallicity tail becomes $\simeq 20 \text{ km s}^{-1}$ when $\mu_{\text{dist}} = 0.8$, while this value becomes $\simeq 70 \text{ km s}^{-1}$ when $\mu_{\text{dist}} = 1.2$ (see Figure 7). The fact that both the G- and K-type dwarfs exhibit $\langle V_\phi \rangle_{\text{med}} \simeq 50 \text{ km s}^{-1}$ at the low-metallicity tail in Figure 1(c) suggests that there is no spectral-type dependence in μ_{dist} in our sample. Therefore, we conclude that the observed offset in the $\langle V_\phi \rangle_{\text{med}}\text{--}[\text{Fe}/\text{H}]$ relation [Figures 1(c) and 2(b)], or the non-existence of it [Figure 2(a)], are not due to observational errors in $[\text{Fe}/\text{H}]$ or distance.

REFERENCES

- Aihara, H., Allende Prieto, C., An, D., et al. 2011, *ApJS*, 193, 29
Allende Prieto, C., Sivarani, T., Beers, T. C., et al. 2008, *AJ*, 136, 2070
An, D., Pinsonneault, M. H., Masseron, T., et al. 2009, *ApJ*, 700, 523
Beers, T. C., Carollo, D., Ivezić, Ž., et al. 2012, *ApJ*, 746, 34
Bondi, H. 1952, *MNRAS*, 112, 195
Bovy, J., Allende Prieto, C., Beers, T. C., et al. 2012, *ApJ*, 759, 131
Bromm, V., Ferrara, A., Coppi, P. S., & Larson, R. B. 2001, *MNRAS*, 328, 969
Caffau, E., Bonifacio, P., François, P., et al. 2012, *A&A*, 542, A51
Carollo, D., Beers, T. C., Lee, Y. S., et al. 2007, *Nature*, 450, 1020
Carollo, D., Beers, T. C., Chiba, M., et al. 2010, *ApJ*, 712, 692
Chiba, M., & Beers, T. C. 2001, *ApJ*, 549, 325

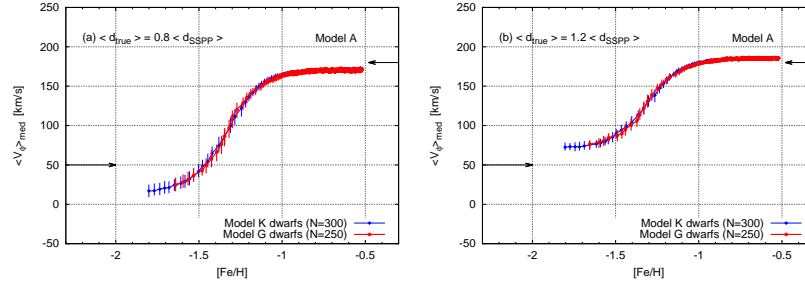


FIG. 7.— The same as in Figure 4(a), but for $\mu_{dist} = 0.8$ (left-hand panel) and $\mu_{dist} = 1.2$ (right-hand panel).

- Chiba, M., & Beers, T. C. 2000, *AJ*, 119, 2843
Christlieb, N., Bessell, M. S., Beers, T. C., et al. 2002, *Nature*, 419, 904
Dehnen, W., & Binney, J. J. 1998, *MNRAS*, 298, 387
Font, A. S., Benson, A. J., Bower, R. G., et al. 2011, *MNRAS*, 417, 1260
Frebel, A., Aoki, W., Christlieb, N., et al. 2005, *Nature*, 434, 871
Frebel, A., Johnson, J. L., & Bromm, V. 2009, *MNRAS*, 392, L50
Ghez, A. M., Salim, S., Weinberg, N. N., et al. 2008, *ApJ*, 689, 1044
Gilmore, G., & Reid, N. 1983, *MNRAS*, 202, 1025
Habets, G. M. H. J., & Heintze, J. R. W. 1981, *A&AS*, 46, 193
Iwamoto, N., Umeda, H., Tominaga, N., Nomoto, K., & Maeda, K. 2005, *Science*, 309, 451
Kerr, F. J., & Lynden-Bell, D. 1986, *MNRAS*, 221, 1023
Komiya, Y., Habe, A., Suda, T., & Fujimoto, M. Y. 2010, *ApJ*, 717, 542
Koposov, S. E., Rix, H.-W., & Hogg, D. W. 2010, *ApJ*, 712, 260
Lee, Y. S., Beers, T. C., Sivarani, T., et al. 2008a, *AJ*, 136, 2022
Lee, Y. S., Beers, T. C., Sivarani, T., et al. 2008b, *AJ*, 136, 2050
Li, H. N., Christlieb, N., Schörck, T., et al. 2010, *A&A*, 521, A10
McCarthy, I. G., Font, A. S., Crain, R. A., Deason, A. J., Schaye, J., & Theuns, T. 2012, *MNRAS*, 420, 2245
Mengel, J. G., Demarque, P., Sweigart, A. V., & Gross, P. G. 1979, *ApJS*, 40, 733
Nakamura, F., & Umemura, M. 2001, *ApJ*, 548, 19
Nomoto, K., Kobayashi, C., & Tominaga, N. 2013, *ARA&A*, 51, 457
Norris, J. E., Christlieb, N., Korn, A. J., et al. 2007, *ApJ*, 670, 774
Safrank-Shrader, C., Bromm, V., & Milosavljević, M. 2010, *ApJ*, 723, 1568
Schlegel, D. J., Finkbeiner, D. P., & Davis, M. 1998, *ApJ*, 500, 525
Schlesinger, K. J., Johnson, J. A., Rockosi, C. M., et al. 2012, *ApJ*, 761, 160
Schörck, T., Christlieb, N., Cohen, J. G., et al. 2009, *A&A*, 507, 817
Sesar, B., Jurić, M., & Ivezić, Ž. 2011, *ApJ*, 731, 4
Shigeyama, T., Tsujimoto, T., & Yoshii, Y. 2003, *ApJ*, 586, L57
Silk, J. 1977, *ApJ*, 211, 638
Simon, J. D., & Geha, M. 2007, *ApJ*, 670, 313
Smith, B. D., Turk, M. J., Sigurdsson, S., O'Shea, B. W., & Norman, M. L. 2009, *ApJ*, 691, 441
Smolinski, J. P., Lee, Y. S., Beers, T. C., et al. 2011, *AJ*, 141, 89
Sollima, A., Bellazzini, M., Smart, R. L., et al. 2009, *MNRAS*, 396, 2183
Stanford, L. M., Da Costa, G. S., Norris, J. E., & Cannon, R. D. 2007, *ApJ*, 667, 911
Suda, T., Aikawa, M., Machida, M. N., Fujimoto, M. Y., & Iben, I., Jr. 2004, *ApJ*, 611, 476
Sweigart, A. V., & Gross, P. G. 1978, *ApJS*, 36, 405
Tissera, P. B., Scannapieco, C., Beers, T. C., & Carollo, D. 2013, *MNRAS*, 432, 3391
Umeda, H., & Nomoto, K. 2003, *Nature*, 422, 871
Walker, M. G., Mateo, M., Olszewski, E. W., et al. 2009, *ApJ*, 704, 1274
Xue, X.-X., Rix, H.-W., Yanny, B., et al. 2011, *ApJ*, 738, 79
Yanny, B., Rockosi, C., Newberg, H. J., et al. 2009, *AJ*, 137, 4377
Yong, D., Norris, J. E., Bessell, M. S., et al. 2013, *ApJ*, 762, 27
Yoshii, Y. 1981, *A&A*, 97, 280
Yoshii, Y. 1982, *PASJ*, 34, 365
Yoshii, Y., & Arimoto, N. 1987, *A&A*, 188, 13
Yoshii, Y., & Sabano, Y. 1980, *PASJ*, 32, 229
Yoshii, Y., & Saio, H. 1986, *ApJ*, 301, 587
Yoshii, Y. 2013, in *Planets, Stars and Stellar Systems. Volume 5: Galactic Structure and Stellar Populations*, eds. T.D. Oswalt, and G. Gilmore, (Springer, Dordrecht), p.395